pp 1-14 Printed in Nigeria

NUMERICAL SIMULATION OF OUTDOOR AIR FLOW AND VENTILATION PERFORMANCE AROUND AN ARRAY OF BUILDINGS

Ayo Samuel Adinoyi[1*], Normah-Mohd Ghazali[2]

[1]Department of Mechanical Engineering, Federal University of Technology Minna, Nigeria
[2]School of Mechanical Engineering, Faculty of Engineering, Universiti Teknologi Malaysia, 81310 Johor Bahru, Johor, Malaysia

Corresponding Email: saayo1@gmail.com

ABSTRACT

This study examines outdoor air flow and ventilation around an array of buildings by parameterizing the separation distance (W) between the frontal column of buildings and the rest of the building array. The aim was to assess the impact of the separation distance on the air ventilation performance. The study was set around a neighborhood of Kuala Lumpur, the Capital City of Malaysia, and employs the numerical simulation technique utilizing the Reynolds Averaged Navier-Stokes equations. The full-scale size models of common building configurations and weather data around the city were utilized to calculate the mean wind field around the building array. The air ventilation performance was evaluated in terms of air velocity ratio (VR) and air flow rate (AFR). Results indicate that the invigoration of the flow in the lateral streets is mostly due to corner-stream inflow into the streets through the side-openings. The VR was found to increase with increase in the separation distance and this was found to be mainly due to corner-stream inflow to the streets. The increase in VR ranged between 15% and 60% between the values at separations W = 12 m and W = 36 m. The results demonstrate the existence of an optimal location of the frontal column of buildings in a building array that would invigorate the outdoor air flow and improve human thermal comfort.

Keywords: Building array; Numerical simulation; Outdoor air ventilation; Velocity ratio, Air flow rate

1. INTRODUCTION

In low-wind urban areas, improving air flow and ventilation around buildings is very important for the thermal comfort and environmental health of the inhabitants. Several researches has, thus, been used to examine strategies which improve air flow and ventilation around building clusters. Air movement is a direct factor of human thermal comfort as it affects the rate at which heat is transferred from the surface of the human skin by convection and evaporation to the environment. Air ventilation, on the other hand, engenders dilution and exchange of domestic anthropogenic heat and pollutant emissions due to vehicular and domestic activities in the urban environment with the cleaner upper atmosphere to improve thermal comfort (Chen et al., 2017; You et al. 2018).

It has been demonstrated that factors which strongly influence air flow and ventilation in street canyons of building arrays include

building packing density (Buccolieri et al, 2010; Buccolieri et al, 2015; Chen et al, 2017), building arrangement (Yim et al, 2009; Yang et al, 2016; You et al, 2018), and direction of ambient wind (van Hooff and Blocken, 2010; Park, 2013; Gough et al, 2018). In other heat generating systems too, it has also been shown that the arrangement of the elements is a crucial factor affecting the rate of heat dissipation (Wulamdari et al, 2020). The application of building density in enhancing air flow and ventilation around building arrays, however, appears to be the most common strategy normally adopted. Unfortunately, the strategy usually involves additional land resource utilization in order to provide the low building density required to engender improved ventilation. This is due of the extra parcel of land that is required in spacing each building in both the longitudinal and lateral directions. On the other hand, if advantage is taken of corner-streams (Penwaden & Wise, 1975) resulting from high-speed winds generated at the base of buildings when an approach wind is intercepted on the buildings' façades, higher street canyon ventilation performance could be achieved with much higher building density. From literatures, it has been observed that this potential and the mechanism by which it occurs have not been adequately explored. It is, thus, the main focus of this study to examine air flow and ventilation around a regular building array by parameterizing the separation distance between the frontal column of buildings and the remaining section of the array and determine how the separation distance can be used to engender higher air flow and ventilation. The lateral passage width between the buildings and the longitudinal distance separating the buildings in the downwind section of the building array are fixed, as such the additional cost incurred by this strategy is that of the marginal increase in the size of the parcel of land between the frontal buildings and the building array downwind.

2. METHODOLOGY OF THE RESEARCH

2.1. Physical Model and Configurations of the Building Layout

The study was conducted with special reference to a low-wind, hot and humid sub-urban area of Kuala Lumpur, the Capital City of Malaysia. Consequently, reference was made to the meteorological conditions of the city and common building configurations found around the city. The meteorological data collected from Subang Meteorological Station situated at a distance of about 23.64 km from Kuala Lumpur Sentral indicate that Kuala Lumpur has a ten-year mean surface wind speed of about 1.52 m/s and an overall 24-hour mean temperature of about 27.77°C. The maximum and minimum mean relative humidity readings are 98% and 38%, respectively. A common residential building style found around Malaysia is building grouping consisting of low-rise buildings, with height equivalent to that of a four-story building. The study employs a 4 x 3 in-line array of the buildings with each of the buildings having dimensions of the building envelope 40 m x 12 m x 10 m in width (W), height (H), and depth (D), respectively. The dimensions of the room units are in accordance with the Bye-Law 42 of Malaysian Uniform Building Bye-Law (UBBL) 1984.

To examine the air flow and ventilation impact of the separation distance on the building array, five different configurations of the array are formed by varying the longitudinal separation distance between the frontal building column and the remaining 3 x 3 array from a minimum of 12 m = H to a maximum of 36 m = $3H$ by a step increase of 6 m = $\frac{1}{2}H$. The 3 x 3 array has a constant longitudinal separation distance W_c = 18 m based on a previous

study. A constant lateral passage width w = 6 m between the buildings is maintained based on Malaysia GP022 Planning Guidelines. The layout and geometries of the building array are as shown in Figures 1 and 2, respectively.

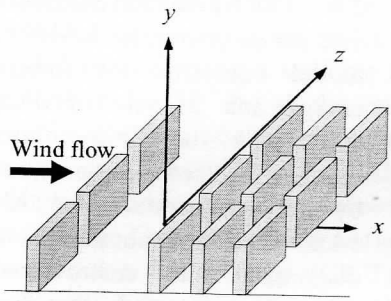

Figure 1 Layout of the building array

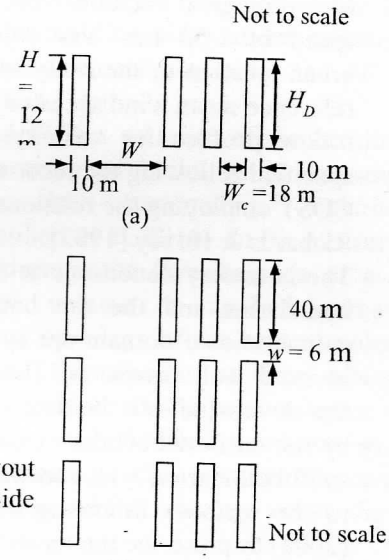

Figure 2 Geometry of the layout of the building array, (a) Side view, (b) Top view

2.2. Approach to the Study and Procedure

The study employs a numerical solution procedure of the computational fluid dynamics (CFD) technique to examine the flow field around the full-scale sizes of the array of buildings. The flow in the urban boundary layer model can be described by the conservation laws of fluid flow. The flow is often considered turbulent at Reynolds number $Re_H \geq 3400$ (Hoydysh, 1974). In the present study, the Reynolds number is determined as $Re_H = 695924.92$, confirming that the flow is in the turbulent regime. The solution procedure adopted is based on Reynolds-Averaged Navier-Stokes (RANS) equations, with closure obtained for the governing equations by the Realizable k-ε turbulence model (Shih et al, 1995), where k is turbulence kinetic energy and ε is the dissipation rate of the kinetic energy. For an isothermal condition of the environment, the governing equations are as expressed by Ayo et al, (2015).

2.3. Configuration of the Computational Domain and Boundary Conditions

To implement the numerical solution of the model equations for the flow around the buildings, a computational domain was designed following recommendations of major guidelines and past studies (Tominaga et al, 2008). In the present study, the inflow boundary is located at a distance $5H$ away from the windward face of the first building at the upwind location, while the outflow boundary is set at $15H$ from the leeward face of the last building at the downwind location. The lateral and top boundaries of the domain are set at $5H$ away from the lateral and the top surfaces of the building, respectively.

The profiles of x-, y- and z-components of velocity, the turbulence kinetic energy, the dissipation rate of the kinetic energy, their gradients and the gradient of pressure are specified at the boundaries of the computational domain as the boundary

conditions. At the inflow boundary, the vertical profile of velocity prescribed is based on the wind data of Subang Meteorological Station. The mean wind speed of 1.52 m/s was adjusted for the urban location of the study area to obtain a reference mean wind speed of 0.92 m/s. The inflow profiles for velocity, k and ε are specified following the recommendations of COST employing the relations suggested by Richards & Hoxey (1993).

The boundary conditions at the two lateral boundaries and the top boundary of the computational domain are specified by the inviscid wall condition. The conditions at the downwind exit boundary are specified by the outflow boundary conditions. At the solid boundaries, wall-functions are applied to the surfaces following Tominaga et al (2008) to prescribe the mean velocity, k and ε conditions at the wall-adjacent cells as follows:

$$\frac{U_p}{u^*} = \frac{1}{\kappa} ln\left(\frac{u^* y_p}{\nu}\right) + B; \quad k_p = \frac{u^{*2}}{\sqrt{C_\mu}}; \varepsilon_p = \frac{u^{*3}}{\kappa y_p} \quad (1)$$

where U_p, k_p, ε_p are, respectively, the tangential component of wind velocity, the k and ε at the centre-point P of the near-wall cell, and y_p is the distance between point P and wall. B ($\approx 5 - 5.5$) is a universal constant, $u^* = C_\mu^{1/4} k_p^{1/2}$, C_μ ($= 0.09$) is a model constant of the Standard k-ε model, ν is the kinematic viscosity of the fluid and κ ($\approx 0.4-0.42$) is von Karman constant. For the rough ground surface, the wall-function for mean velocity of the wall-adjacent cells is expressed as (ANSYS Fluent 14.0, 2011),

$$\frac{U_p}{u^*} = \frac{1}{\kappa} ln\left(\frac{u^* y_p}{\nu C_S K_S^+}\right) + 5.43 \quad (2)$$

where $K_S^+ \left(= \frac{u^* K_S}{\nu}\right)$ is the dimensionless surface roughness height, $K_S \left(= \frac{9.793 y_0}{C_S}\right)$ is the dimensional roughness height, and C_S, with value in the interval between 0 and 1, is the surface roughness constant which accounts for the type of roughness.

2.4. The Numerical Simulation

The set of governing RANS equations and model equations for turbulence kinetic energy and its rate of dissipation were solved by the finite-volume numerical method. The computation was implemented by the commercial code ANSYS Fluent 14.0. The computational domain was discretized into unstructured tetrahedral grid elements, with the finest elements concentrated around building corners and in the vicinity of solid surfaces. Far from the solid surfaces the mesh elements are larger, gradually increasing from the surfaces by expansion ratios not greater than 1.2. The aspect ratios of the elements range between 0.5 and 20 (ANSYS Fluent 14.0, 2011).

The pressure-based solver which adopts the Semi-Implicit Method for Pressure-Linked Equations (SIMPLE) algorithm to solve the pressure-velocity coupling was used in computing the mathematical models. At the inflow boundary, user defined function (udf) was used in coding the profiles for U, k and ε to implement the flow conditions at the boundary in the solver. At the lateral and top boundaries of the domain, the prescribed flow conditions were implemented in the solver by specifying zero shear stress condition, while at the downstream boundary, the flow conditions were implemented by the outflow boundary conditions. For the ground surface, equation (2) was implemented in the solver to calculate the values of the mean velocity at the wall-adjacent cells, while equation (1) was implemented to calculate the values for k and ε at the cells. The ground terrain roughness height $y_0 = 0.02\ m$, corresponding to a grassland terrain with grass cover varying between short and long grass (Wieringer, 1992) and a roughness constant C_s = 1.0 were specified to be able to calculate the values of the wall-adjacent

variables. The wall-function for a smooth surface as expressed by equation (1) was implemented in the solver for the building surfaces. During the computation, convergence of the iteration process was controlled by specifying a uniform scaled-residual set at 1 x 10^{-5} for all the variables. The implementation of the computation of the model equations was accomplished on the High-Performance Computer (HPC) system of the Centre for Information and Communication Technology (CICT) Unit of Universiti Teknologi Malaysia (UTM), Malaysia.

2.5. Air Ventilation Performance Indicators

The air ventilation performance criteria adopted for the various configurations of the building array examined are air velocity ratio (*VR*) and air flow rate (*AFR*). The *VR* is a dimensionless quantity of the ratio of wind speed at the pedestrian level (2 m height) around a building to the freestream wind speed at the boundary layer height. For the building array under investigation, the measurement planes for the *VR* are as shown in Figure 3.

The *AFR* is a measure of the breathability of an array of buildings to exchange air with the surrounding environment (Buccolieri et al, 2010). In the measurement procedure, mass flow balance of a target control volume is applied across the external openings of the control volume to estimate the amount of flow across the control volume. In the present layout of the building array, the control volume, which is the domain of the downstream array of buildings, and the openings are as shown in Figure 4.

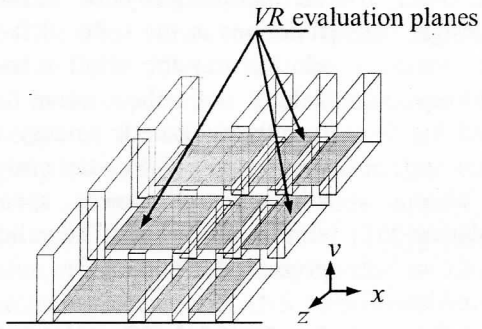

Figure 3 *VR* evaluation planes for the building array

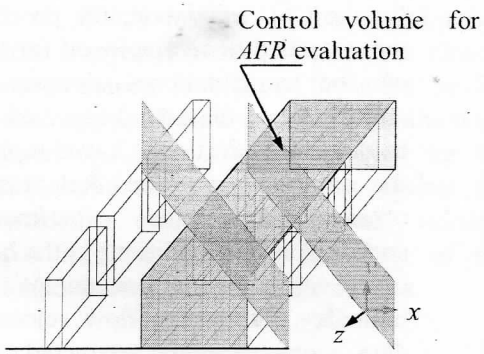

Figure 4 *AFR* evaluation geometries for the building array

The *AFR* normalized with the flow rate referenced at a location far upwind where flow conditions are not disturbed by the presence of the buildings can be expressed as

$$q^* = \frac{q}{q_{ref}} = \frac{\int_A \vec{V}.\vec{n}dA}{\int_A \vec{U}_{ref}.\vec{n}dA} \quad (3)$$

where $\vec{V}$ and $\vec{n}$ are respectively the velocity vector and the unit vector normal to the surface of an opening, and A is the area of the opening. $\vec{U}_{ref}.\vec{n}$ is streamwise velocity at the far upwind location of the building array through an area A with size equivalent to the area of the frontal openings. Equation 3 was used to estimate the air flow rate across the external openings of the building array.

2.6. Validation of the CFD Turbulence Model

In order to ascertain that the RKE turbulence model was robust enough to satisfactorily simulate the flow field around the building array, the validation of the model was performed. This was done by

predicting, using the turbulence models, the flow field around an array of scaled-models of city blocks employed in a wind tunnel experiment conducted at the Japanese National Institute for Environmental Studies (Uehara et al., 2000) and comparing the simulation results with data from the experiment. Several research studies have employed data from this experiment in the past for similar validation purposes (Xie et al, 2007). The model city blocks and measurement geometries were set as shown in Figure (5) (Uehara et al, 2000).

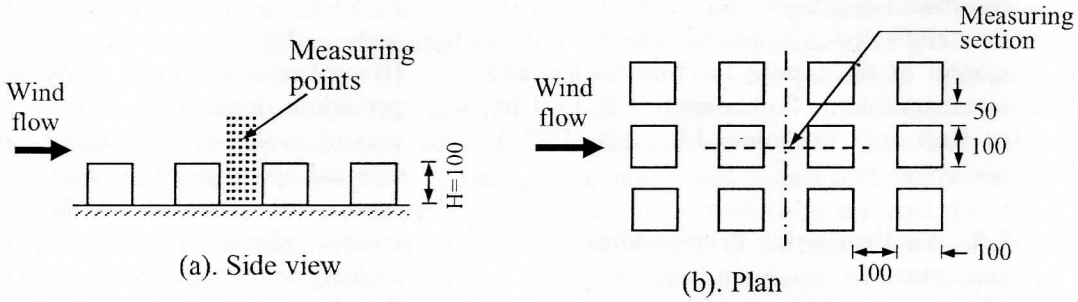

Figure 5 Setting of experimental models and the measurement points (in mm)

In the design of the computational domain for the CFD validation, the procedure that was intended to be employed for the design of the computational domain for the simulation of the actual array of buildings as detailed in section 2.2 was replicated for the validation exercise. Relevant data as obtained from the experiment were specified as the conditions at the boundaries of the computational domain. At the inflow boundary, the mean inflow velocity profile data were carefully extracted from the graphical results provided in the literature and fitted with closely approximating curves to serve as the mean wind speed profile at the inflow boundary. The velocity variance and the turbulence kinetic energy were obtained from the friction velocity, the roughness length and roughness Reynolds number, and the scaled velocity variances all of which were also provided in the literature for the approach flow. The profile of the rate of dissipation of turbulence kinetic energy at the inflow boundary was specified as expressed by Richards & Hoxey (1993). At the other boundaries of the computational domain, conditions were specified as were done for the simulation of the actual array of buildings. The wall functions at the solid surfaces of the model blocks and the wind tunnel floor for the values of the mean flow velocity, turbulence kinetic energy and the rate of dissipation of kinetic energy at the wall-adjacent cells were specified following similar procedure. The validation results are presented in section 3.

3. RESULTS AND DISCUSSION

3.1. Results of the CFD Validation

The results of the CFD validation of the Realizable k-ε turbulence model employed in this study are presented in this section. But first, a comparison is made between the profile of the approximating function of the data of the approach flow measured in the wind tunnel experiment employed for the CFD validation and the profile of the data as shown in Figure 6. The figure demonstrates that the approximating function employed for the wind speed data at the inflow boundary closely follows the profile for the measured wind speed data. The results gave the authors the confidence

that the right profile of the approach flow has been specified for the CFD validation exercise and therefore proceeded to conduct the validation. The CFD validation result is presented in Figure 7.

In Figure 7 the measured vertical profile of the normalized streamwise velocity component at the center of the target street canyon is compared with the calculated values. The figure shows that the simulation result of the vertical profile of the streamwise velocity component has the same pattern as that of the experimental data. It is also shown in the figure that the result closely agrees with the experimental data, particularly at the higher wind region, i.e. at $y/H \geq 1.0$. It would also be observed from the figure that the in-canyon recirculation vortex observed in the experiment is satisfactorily reproduced by the simulation. It is observed, however, that in the weak wind region, particularly for $y/H < 1.0$, the mean wind speed is calculated a little lower than the values measured in the experiment. The calculation of the centre of the recirculation vortex is also slightly lower than that measured in the experiment. However, these results are consistent with those of Yim et al (2009) and Yoshie et al (2007) and may be due to the inherent weakness of RANS turbulence models to accurately predict the flow field in the wake region. The uncertainty with some of the conditions imposed at the boundaries, such as the profiles for k and ε, and the surface roughness at the solid boundaries, might have also contributed to the observed discrepancy. It is believed that utilizing actual values of these boundary conditions would significantly improve the prediction accuracy of the RKE turbulence model.

When compared to the results of previous validation (Xie et al., 2007) conducted for the unstable condition of the atmosphere, the results for the present study have been demonstrated to yield a much better performance. This may be as a result of the actual 3-D configuration adopted for the present validation compared to the 2-D configuration used in these previous studies or the isolated street canyon employed (Xie et al., 2005) instead of the actual urban street canyon involved. Besides, a closely approximating function of the actual profile of the approach flow at the inlet of the wind tunnel test section was employed for the CFD validation simulation as against the vertically uniform horizontal velocity prescribed at the inlet boundary of the computational domain in the studies.

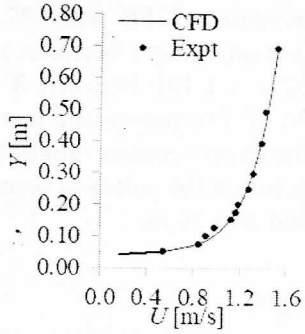

Figure 6 Measured approach flow vertical wind profile and the CFD approximation

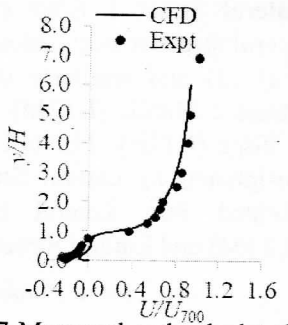

Figure 7 Measured and calculated vertical profiles of normalized streamwise velocity component at the center of the target street

Considering the overall satisfactory performance of the model, it was believed that the model is robust enough in realistically predicting the flow field around

the array of buildings under investigation. The air ventilation performance of the different configurations of the building array was, thus, proceeded with to be examined by the turbulence model.

3.2. Results for the Array of Buildings

Results are hereby presented for the air ventilation performance of the flow around various configurations of the regular building array examined. The ventilation performance was measured in terms of air velocity ratio and dimensionless air flow rate, and are presented for the various sections of the streets. But first, the street sections were each designated for the half-domain configuration of the building array as shown in Figure (8), for the purpose of easy identification. In the figure, ten different street sections consisting of nine lateral street sections and a streamwise street section were identified. The street along the direction of flow was designated Longitudinal Street (LG). The lateral street that separates the frontal column of buildings and the remaining array is called Lateral Street 1 (LT1). The street is divided into the portion by the middle of the building array, called Lateral Street 1 Middle (LT1M), and the portion towards the side of the building array and called Lateral Street 1 Edge (LT1E). The next lateral street is designated as Lateral Street 2 (LT2) and similarly divided as Lateral Street 2 Middle (LT2M) and Lateral Street 2 Edge (LT2E). The last lateral street was designated as Lateral Street 3 (LT3) and divided into Lateral Street 3 Middle (LT3M) and Lateral Street 3 Edge (LT3E).

Figure 9 shows the profiles of velocity ratio at the pedestrian level for various sections of the streets of the building array, while the average velocity ratio characteristics for the measurement planes is shown in Figure 10. Figure 9 shows that *VR* is not uniform across the streets. The *VR* is higher at LT1 than at LT2 and LT3, and at the edge sections than the middle sections. It is highest at LT3E and least at LT3M for all separation distances except at *W* between 24 m and 36 m, with a maximum percentage difference ranging between 146% at $W = 12$ m and 214% at $W = 24$ m. At the edge sections, the *VR* is highest at LT3E and least at LT2E, while at the middle sections, it is highest at LT1M and least at LT2M and LT3M.

The *VR* at the street sections generally increases with increase in separation distance between the frontal column of building array and the objective domain, except at LT2M where it decreases continuously with increase in the separation distance. The *VR* increases continuously with increase in separation distance for the edge sections of the objective domain, while for the separation streets the *VR* increases with the distance until it reaches a maximum, after which it begins to decrease with further increase in the separation. The increase of *VR* with *W* across the street sections ranges between 15% at LT1E and 62% at LT2E between $W = 12$ m and $W = 36$ m. The percentage increase in *VR* across the street sections ranges from 15% to 60% between the values at separations $W = 12$ m and $W = 36$ m.

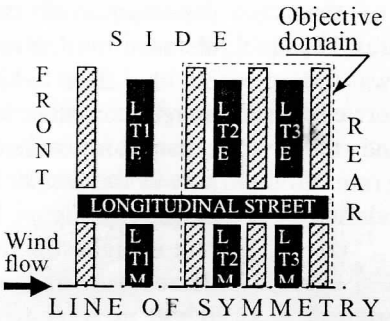

Figure 8 Street designations for half-domain in top view

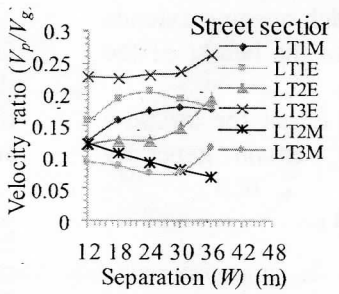

Figure 9 Profiles of velocity ratio at various street sections of the building array

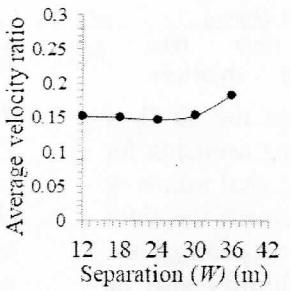

Figure 10 Profile of average velocity ratio

Figure 10 shows that the average velocity ratio characteristics across the whole pedestrian-level planes tends to be invariant with separation distance until as from W = 24 m when the VR begins to increase with increase in the separation distance. The increase in in the average VR is about 21% between the values at W = 12 m and W = 36 m.

The air flow rate characteristics of the objective domain are shown in Figures 11, 12 and 13. While Figure 11 shows the impact of the separation distance between the frontal column of building and the objective domain on the overall (net) rate of air exchange across the domain boundaries, Figure 12 shows the flow rate characteristics through the front, sides, top and rear openings of the domain in order to examine the contribution of air exchanges across each opening of the domain. Figure 13, on the other hand, shows the flow balance and the direction of flow across the various openings of the objective domain for various separation distances. The entry path into the array for each opening extends from the ground level to the height of the buildings.

It is shown in Figure 11 that the air flow rate for the objective domain generally decreases with increase in the separation distance until it reaches a minimum at W = 30 m, after which it begins to mildly increase with further increase in the separation distance. The result is similar in part to the results observed in Buccolieri et al. (2010). Figure 12 shows that the air flow rate is highest across the top opening, but it decreases with separation distance until at W=30 m, after which it begins to increase. The flow rate across the front opening decreases with increase in separation distance, while that across the side openings increases with increase in the distance. The flow rate across the rear opening is least of all and, like the flow through the front opening, decreases with separation distance. From Figure 13, it would be observed that the net air flow into the domain is through the front and side openings, while the top and rear openings serve for the net outflow.

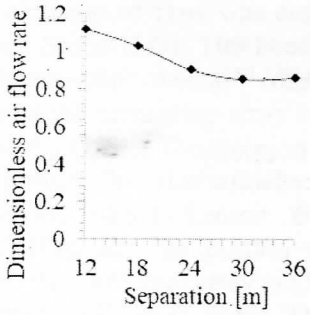

Figure 11 Air flow rate characteristic of the objective

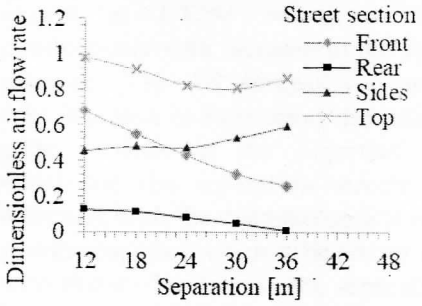

Figure 12 Air flow rate characteristics of the various openings of the domain

Figures 12 and 13 show that the air flow rate through the front opening accounts for the greater proportion of the total inflow at W < 24 m, whereas that through the sides accounts for the greater proportion of the net inflow at W > 24 m. It may also be observed from Figure 12 that the initial rate of decrease of the inflow through the frontal opening is so high that the rate of increase of the inflow through the sides is not sufficient to offset the rate of decrease. The overall rate of air flow into the objective domain, thus, decreases with separation distance until at W = 30 m as observed in Figure 11. In order to understand the flow mechanism responsible for the flow characteristics just observed, an inspection of typical flow patterns around the building array was undertaken.

Figure 14 shows typical flow patterns around some horizontal sections of the half-domain of the building array at the pedestrian height. From the figure, it would be observed that at W = 12 m, there is high-speed inflow through the frontal opening, which extends far into the objective

domain. But as the separation distance increases, the reach of the high-speed inflow decreases and at $W > 24$ m, the high-speed inflow is almost entirely confined to and dispersed into Lateral Street 1. It would also be observed that the inflow through the side openings is mainly due to the high-speed corner-streams. At small separations, e.g. $W = 12$ m, the flow tends to overshoot the openings and therefore the proportion that is intercepted into the objective domain is small.

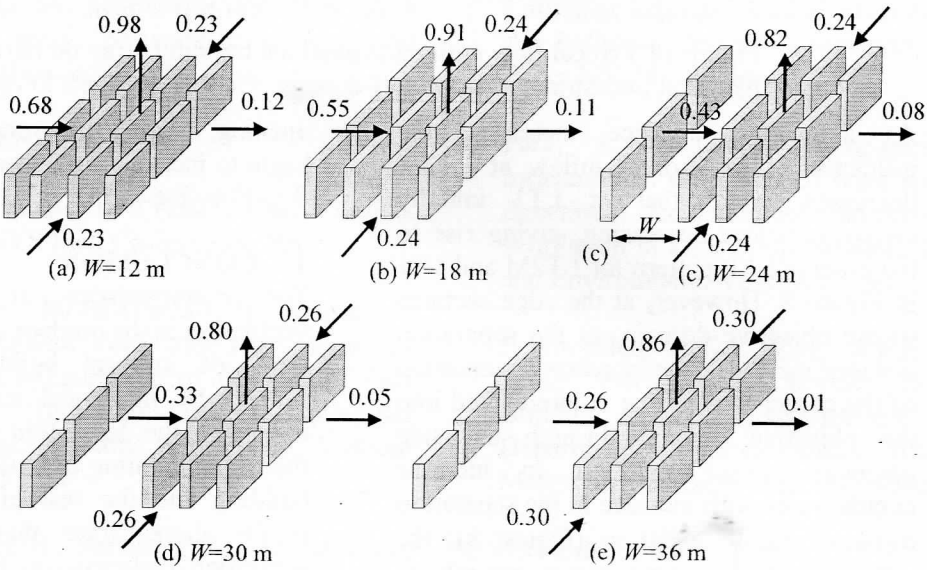

Figure 13 Flow balance and the direction of flow across the various openings of the objective domain for various separation

However, as the separation distance increases, greater proportion of the flow is intercepted into the domain, beginning with LT3 and then LT2. It, thus, indicates that the flows at the middle section of the objective domain, particularly at LT2M, and at LT2 are influenced mainly by the frontal inflow, while those at the edge sections of the objective domain are influenced more by the corner-stream inflow.

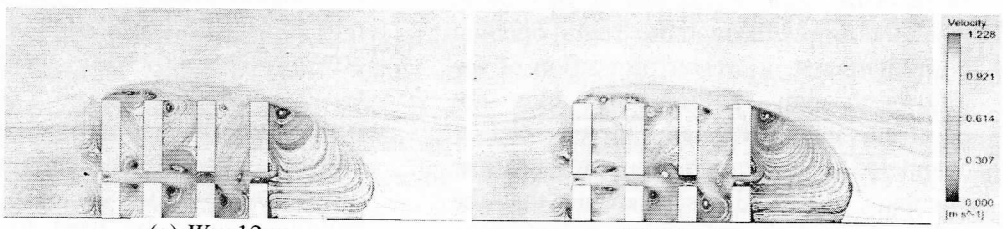

(a) $W = 12$ m (b) $W = 18$ m

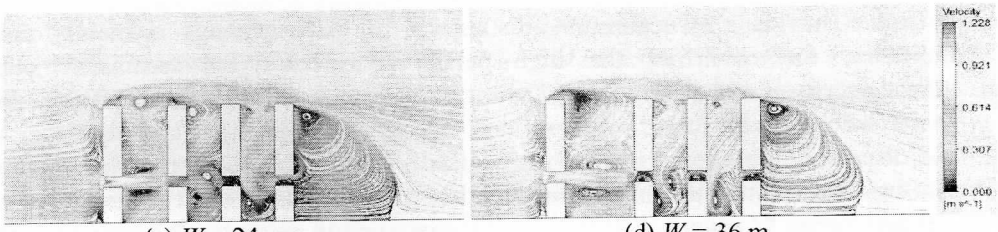

(c) $W = 24$ m (d) $W = 36$ m

Figure 14 Typical flow patterns around the building array on horizontal planes at pedestrian level for half-domain. Flow is from left to right

As separation distance increases, the influence of the frontal inflow at LT2M decreases, while that at LT1 initially increases before decreasing, giving rise to the observed *VR* pattern for LT2M and LT1 in Figure 8. However, at the edge sections of the objective domain, as the separation distance increases, the increasing proportion of the corner-stream that is intercepted into the objective domain through the side openings causes the *VR* to increase continuously with increase in the separation distance. At $W \geq 30$ m (Figure 8), the influence of the corner-steam extends to LT3M, causing the *VR* to rise.

Comparing the results for the velocity ratio shown in Figure 9 and that for the air flow rate, Figure 11, it would be noticed that while the mean wind speeds at various streets, except at LT2M, increases with increase in separation distance, the air flow rate decreases with increase in separation distance before tending to increase for $W \geq 30$ m. This could mean that at $W < 30$ m when the inflow through the frontal opening is predominant, a greater proportion of the inflow through the opening does not penetrate into the lateral streets, but is channeled out through the top and rear openings. It would also indicate that the inflow through the side openings invigorate the pedestrian wind flow more than that through the frontal opening. This is observed from Figure 12 in which the rapid increase in the air flow rate through the side openings after $W = 24$ m is able to offset the decrease in the inflow through the frontal opening, causing the overall air flow rate to begin to increase with separation distance at $W = 30$ m (Figure 11).

4. CONCLUSION

The characteristics of air flow and ventilation at the outdoor environment of an array of uniform buildings have been studied by numerical simulation for the effects of the separation distance between the frontal column of buildings of a regular building and the rest of the arrays. The results demonstrate that increasing the separation distance can trigger significant increase in the mean wind speeds at almost all sections of the streets. The invigoration of the wind motion is mostly due to the inflow across the lateral street openings, which tends to increase with separation distance. The inflow through the frontal opening contributes very little to the invigoration of the wind motion in the lateral streets. However, the breathability of the neighbourhood as depicted by air flow rate across the boundaries of the building array decreases with increase in the separation distance. It is, therefore, concluded that the separation distance between the frontal buildings and the downwind part of an array of uniform buildings could be used to significantly enhance air flow and thus, thermal comfort, for residential neighbourhoods in which there exists little or no vehicular emissions, or other noxious gases in the environment. Further studies could be carried out to examine the impact of the width of the

Longitunal Street on the ventilation parameters, which appears in the present study to be insignificant probably due to the narrow width specified. The findings could be applied in the building industry where it would provide a useful strategy for enhancing air ventilation and flow in a building array, particularly in low-wind residential environments.

REFERENCES

ANSYS Fluent 14.0 (2011) User's Guide. ANSYS Inc., Canonsburg, PA.

Ayo, S.A., Mohd-Ghazali, N., Mansor, S (2015) Outdoor Ventilation Performance of Various Configurations of a Layout of Two Adjacent Buildings under Isothermal Conditions. Building Simulation. Volume 8(1), pp. 81-98

Buccolieri, R., Sandberg, M., Di Sabatino, S (2010) City Breathability and its Link to Pollutant Concentration Distribution within Urban-like Geometries. Atmospheric Environment. Volume 44 (15), pp. 1894-1903.

Buccolieri, R., Salizzoni, P., Soulhac, L., Garbero, V. Di Sabatino, S (2015) The breathability of compact cities. Urban Climate. Volume 13, pp. 73 – 93.

Chen, L., Hang, J., Sandberg. M., Claesson, L., Di Sabatino, S (2017) The influence of building packing densities on flow adjustment and city breathability in urban-like geometries. Procedia Engineering. Volume 98, pp. 758 – 769.

Gough, H., Sato, T., Halios, C., Grimmond, C. S. B., Luo, Z., Barlow, J. F., Robertson, A., Hoxey, R., Quinn, A (2018) Effects of variability of local winds on cross ventilation for a simplified building within a full-scale asymmetric array: Overview of the Silsoe field campaign. Journal of Wind Engineering & Industrial Aerodynamics. Volume 175.

Hoydysh, W.A (1974). Scale Model Study of Dispersion of Pollutant in Street Canyons. In: 67th Annual Meeting of the Air Pollution Control Association (APCA) Paper No. 74–157. Denver, CO.

Park, J. S (2013). Long-term field measurement on effects of wind speed and directional fluctuation on wind-driven cross ventilation in a mock-up building. Building and Environment. Volume 62, pp. 1 – 8.

Pendwarden, A.D., Wise, A.F.E (1975) Wind Environment around Buildings. Building Research Establishment Report. Department of Environment, BRE, Her Majesty's Stationery Office, London, UK.

Richards, P.J. Hoxey, R.P (1993) Appropriate Boundary Conditions for Computational Wind Engineering Models using the k-ε Turbulence Model. Journal of wind engineering and industrial aerodynamics. Volume 46, pp. 145-153.

Shih, T.H., Liou, W.W., Shabbir, A., Yang, Z., Zhu, J (1995) A New k–ε Eddy Viscosity Model for High Reynolds Number Turbulent Flows. Computers & Fluids, Volume 24, pp. 227–238.

Tominaga, Y., Mochida, A., Yoshie, R., Kataoka, H., Nozu, T., Yoshikawa, M., Shirasawa, T (2008) AIJ Guidelines for Practical Applications of CFD to Pedestrian Wind Environment around Buildings. Journal of Wind Engineering and Industrial Aerodynamics. Volume 96(10), pp. 1749-1761.

Uehara, K., Murakami, S., Oikawa, S., Wakamatsu, S (2000) Wind Tunnel Experiments on How Thermal Stratification

Affects Flow in and above Urban Street Canyons. Atmospheric Environment. Volume 34(10), pp. 1553-1562.

Wieringa, J (1992) Updating the Davenport Roughness Classification. Journal of Wind Engineering and Industrial Aerodynamics. Volume 41(1), pp. 357-368.

Wulandari, D. A., Akmal, M., Gunayan, Y., and Nasruddin (2020). Cooling Improvement of the IT Rack by Layout Rearrangement of the A2 Class Data Center Room: A Simulation Study. EVERGREEN. Volume 07(04), pp. 489-499.

Xie, X., Huang, Z., Wang, J.-S (2005) Impact of Building Configuration on Air Quality in Street Canyon. Atmospheric Environment. Volume 39(25), pp. 4519-4530.

Xie, X., Liu, C.-H., Leung, D.Y.C (2007) Impact of Building Facades and Ground Heating on Wind Flow and Pollutant Transport in Street Canyons. Atmospheric Environment. Volume 41(39), pp. 9030-9049.

Yang, F., Gao, Y., Zhong, K., Khang, Y (2016) Impacts of cross-ventilation on the air quality in street canyons with different building arrangements. Building and Environment. Volume 104, pp. 1-12.

Yim, S.H.L., Fung, J.C.H., Lau, A.K.H., Kot, S.C (2009) Air Ventilation Impacts of the "Wall Effect" Resulting from the Alignment of High-Rise Buildings. Atmospheric Environment. Volume 43(32), pp. 4982-499.

Yoshie, R., Mochida, A., Tominaga, Y., Kataoka, H., Harimoto, K., Nozu, T., Shirasawa, T (2007) Cooperative Project for CFD Prediction of Pedestrian Wind Environment in the Architectural Institute of Japan, Journal of Wind Engineering and Industrial Aerodynamics. Volume 95, pp. 1551–1578.

You, W., Shen, J., Ding, W (2018) Improving residential building arrangement design by assessing outdoor ventilation efficiency in different regional spaces. Architectural Science Review. DOI: 10.1080/00038628.2018.1471388